Imaging Metals in Proteins by Combining Electrophoresis with Rapid X-ray Fluorescence Mapping

Lydia Finney[†,‡,*], Yasmin Chishti[†], Tripti Khare[†], Carol Giometti[†], Aviva Levina[§], Peter A Lay[§], and Stefan Vogt[‡]

[†]Biosciences Division and, [‡]X-ray Sciences Division, Argonne National Laboratory, Argonne, Illinois, and [§]School of Chemistry, The University of Sydney, NSW 2006, Australia

An estimated one-third of all proteins bind metal ions (*1–3*). Essential metal ions, including calcium, iron, copper, and zinc, are imported first into the cell and then further into various cellular compartments, as they are carefully directed into the correct metalloproteins. Exactly how the "right" metal gets to the "right" spot is not well understood, and it is likely to depend on the protein in question. In select pathways, metal homeostasis is accomplished by partner-protein specific metallochaperones (*1, 2*), and these proteins clearly play an important role. Yet, metal ion availability can also exert a controlling influence on the activity of metalloproteins, overriding even the thermo-dynamics of coordination chemistry through the establishment of kinetically trapped states (*3*). In any case, it appears likely that the intracellular distribution and speciation of metals is a dynamic process that is influenced by external stimuli and physiological factors. Recent improvements in our ability to visualize biological metals at the cellular level have brought us a new understanding of the dramatic extent to which the organization of metals within the cell may change during physiological events. For example, copper extensively relocalizes in endothelial cells during the morphogenic process of angiogenesis (*4*), and there are significant changes in elemental distributions and concentrations within aorta endothelial cells when exposed to oxidative stress associated with cardiovascular disease (*5*) and to neurons in models of stroke (*6*).

In addition to the above-mentioned factors, the physiology of metal ion distribution among proteins may be perturbed by metallopharmaceuticals (*7*) and environmental pollutants (*8*). Both types of metal compounds

ABSTRACT Growing evidence points toward a very dynamic role for metals in biology. This suggests that physiological circumstance may mandate metal ion redistribution among ligands. This work addresses a critical need for technology that detects, identifies, and measures the metal-containing components of complex biological matrixes. We describe a direct, user-friendly approach for identifying and quantifying metal−protein adducts in complex samples using native- or SDS-PAGE, blotting, and rapid synchrotron X-ray fluorescence mapping with micro-XANES (X-ray absorption near-edge structure) of entire blots. The identification and quantification of each metal bound to a protein spot has been demonstrated, and the technique has been applied in two exemplary cases. In the first, the speciation of the *in vitro* binding of exogenous chromium to blood serum proteins was influenced markedly by both the oxidation state of chromium exposed to the serum proteins and the treatment conditions, which is of relevance to the biochemistry of Cr dietary supplements. In the second case, *in vivo* changes in endogenous metal speciation were examined to probe the influence of oxygen depletion on iron speciation in *Shewanella oneidensis*.

*Corresponding author,
lfinney@anl.gov.

interact extensively with proteins, including the binding of platinum and ruthenium anticancer drugs to blood serum proteins (7, 9, 10) and detoxification of cadmium and mercury ions by metallothioneins (8). A specific example may be seen in chromium biochemistry (11). Chromium in its highest oxidation state (Cr(VI)) is a recognized human carcinogen (12) and one of the most widespread industrial and environmental pollutants (11). The most stable oxidation state of Cr (Cr(III)), on the other hand, is considered by many nutritionists as an essential trace element involved in glucose metabolism in humans (13), although this has been questioned (14, 15). The balance of toxic and beneficial actions of Cr compounds is likely to be determined by their interactions with biomolecules, primarily proteins and endogenous oxidants (H_2O_2, organic peroxides, *etc.*), both within cells and in the extracellular space (14, 15).

Clearly, in order to understand better the roles of metalloproteins in living systems, it is necessary to understand their chemistry under conditions that are as close to *in vivo* biochemistry as possible, ideally capturing the dynamics of metal occupancy that accompany physiological events. The most straightforward way to visualize the metal−protein interactions is through imaging. Imaging of 2-D electrophoresis gels is a "gold standard" of analysis in proteomics. This could be an ideal initial step to unraveling the challenge of capturing changes in metal occupancy. Yet, up to this point, we cannot image or map the metals bound to proteins separated in this way as readily as we can stain and image the proteins themselves. Many unique challenges exist. The very low levels of metals in typical biological samples demand exceptionally high sensitivity for metal determination. Low-relative-abundance metalloprotein components of complex mixtures may correspond to mere picograms of detectable metal, even when the maximum resolvable protein loads are separated on a given gel.

Several metal detection methods useful at these concentrations exist; these include atomic absorption spectrometry, inductively coupled plasma atomic emission spectroscopy (ICP-AES) and inductively coupled plasma mass spectrometry (ICP-MS) (16, 17). Such techniques are very useful for measuring the total quantity of a metal of interest in a solution sample but typically not the spatial distribution of elements within samples. A notable exception to this is laser-ablation inductively coupled plasma mass spectrometry, in which a laser

source is used to vaporize selectively an area of sample (18–22), thus allowing some spatial discrimination, and some respectable progress has been made to marry these techniques (3, 23). On the other hand, synchrotron X-ray fluorescence microprobe detection (XRF) is remarkably well-suited to the task as a nondestructive technique that provides both high sensitivity and *in situ* sample measurement in a true raster-scan imaging, or mapping, modality with quantitative detection of low-Z elements such as sulfur to enable direct complementary and simultaneous quantification of the proteins themselves (24). Further, it presents the opportunity to interrogate the chemical state of metal cofactors using X-ray absorption spectroscopy (XAS) (25). This precise combination of properties makes it attractive for development as a mapping technique to pair with gel electrophoresis.

Previous experiments have used XRF to identify the positions of metalloproteins on one-dimensional isoelectric focusing materials (16, 26–34) or on native or denaturing polyacrylamide gel electrophoresis (SDS-PAGE) substrates (16, 31–35) to demonstrate the feasibility and sensitivity of this technique. The high-throughput identification of metalloproteins is a long-standing goal (36–38), and advances in imaging or mapping of metals at the cellular level have only reinvigorated interest in its fulfillment. In this context, we now describe an approach that combines metalloprotein-friendly separations with rapid XRF scanning at newly dedicated, publicly available facilities at beamline 8-BM of the Advanced Photon Source at Argonne National Laboratory. The use of these tools to address the interactions of chromium with serum proteins in an *in vitro* setting and to demonstrate the ability to monitor endogenous metals at levels present *in vivo* by observing changes in the speciation of iron during oxygen depletion in *S. oneidensis* are reported.

RESULTS AND DISCUSSION

Observing the Use of Metals: a Mapping Approach. All living systems depend on metalloproteins (1, 2, 16, 17, 39–41). Considering that metals themselves are fluorescent when excited at X-ray energies, we sought to enable combined XRF and XAS characterization of metalloprotein molecules separated by electrophoresis to create a user-friendly and rapid technique for the study of metalloproteins. To this end, a simple but rapid mapping apparatus (Figure 1) was assembled. In this

prototype instrument, undulator-generated hard X-rays were monochromatized and passed through a pinhole. An incident energy of 10 keV was chosen to excite elements up to $Z = 30$ (zinc), but the energy range can be easily adjusted to incorporate higher values to enable detection of higher-Z elements (e.g., Se), at the cost of somewhat reduced sensitivity for the lower-Z elements. Full X-ray fluorescence spectra, including data on all elements from sulfur through zinc, were collected using a single-element detector as the blot was raster-scanned through the X-ray beam. Using this instrument, a native-PAGE separation of metalloproteins (to prevent disruption of metal ion coordination by denaturation) was examined initially to obtain the map shown (Figure 2). The top right panel shows a photograph of the PVDF blot, which includes prestained molecular weight standards, in order to facilitate the visual orientation of the sample at the beamline. Hemoglobin (Hb) bands are visible in this picture due to their natural brown color. Other panels in Figure 2 include selected elemental distribution maps of the blot obtained by XRF mapping, including those for iron, copper, and zinc. Zinc is clearly present in the carbonic anhydrase (CA) band but is not detected in any other bands. Likewise, only hemoglobin contains measurable iron. Copper is present both in the tyrosinase (Tyr) band as well as faintly in two bands of the carbonic anhydrase sample, possibly due to the partial replacement of Zn(II) with Cu(II) during isolation and purification of the protein. Subsequent mapping of a gel containing only a carbonic anhydrase isoform II sample from Sigma showed that it did not contain any copper (as in Figure 3) and migrated as one band. Finally, the far right lane (mix) shows that each metalloprotein may be individually resolved when separated from each other in a mixture.

Perhaps equally critical to the success of this approach was the method of separation that was designed to minimize changes in speciation. As can be seen in Figure 3, classical denaturing SDS-PAGE completely removes the metals from the proteins we tested. Native-PAGE is certainly nothing new, and comparison of results we obtained making our own gels with Milli-Q water did not afford significant advantages over commercially available products. However, all of the equipment used had to be kept rigorously clean and manipulated only with clean plastic tweezers, and unnecessary reductants or chelating agents had to be avoided. Staining techniques, which tend to utilize acidic solutions
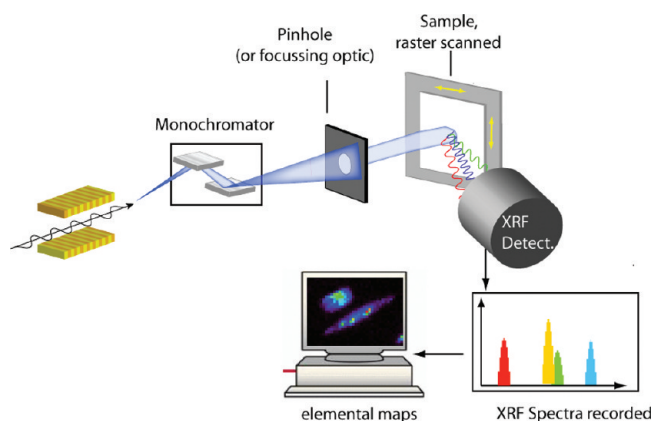

Figure 1. Prototype instrument for XRF scanning of electrophoretic separations. Undulator generated X-rays are monochromatized and passed through a pinhole. The sample was raster-scanned through the X-ray beam, and emitted X-ray fluorescence was collected at 90°. The signal was then deconvolved pixel-by-pixel to produce elemental maps of the sample for each metal. The abbreviation MW is used to mark lanes where molecular weight marker was applied.

that may disrupt the coordination of metal ions, were entirely avoided prior to mapping by XRF. We found significant advantages to mapping blots over mapping the gels themselves. Not only does the PVDF provide a lower background level of fluorescence, but it is stringently flat, making it possible to keep the sample to detector distance constant during scanning (and thus avoid potential artifacts in metal quantification).

It may be argued that native separations do not provide adequate resolution in some situations. Certainly, the use of detergent (SDS), reductants, and chelating agents to remove the influence of shape and charge on separation has its advantages. As we continue to study the way that metalloprotein complexes are affected by separation methods, we hope to find ways to address further the difficult task of separating proteins from each other without separating them from their metals. In the case of interactions of chromium with serum proteins, described in detail later, some improvements in resolution with minimal loss of chromium were achieved through the addition of SDS alone. It is likely that we were able to observe this interaction despite the presence of SDS because these exogenous metal compounds bind adventitiously to exposed donor groups on the surface of the protein (42). Approaches like this may be useful in other cases.
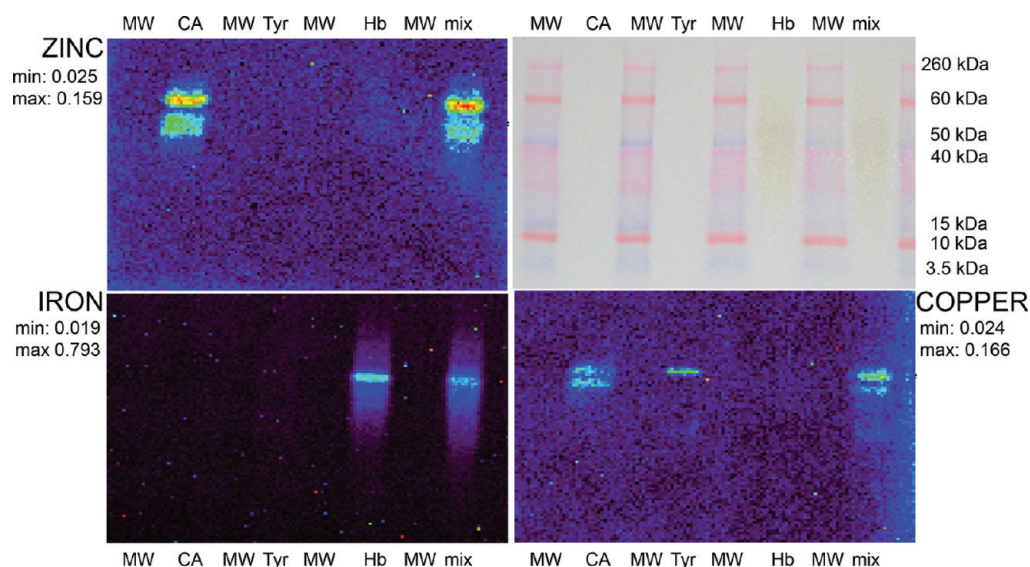
Figure 2. XRF map of a one-dimensional native-PAGE blot of multiple metalloproteins. (Upper right) Photograph of blot. (Upper left) Zinc map shows zinc present in carbonic anhydrase (CA). (Lower left) Iron map shows iron present in hemoglobin (Hb). (Lower right) Copper map shows copper present in tyrosinase (Tyr), as well as a contaminant in carbonic anhydrase. Maps displayed are quantified, with threshold values in $\mu g/cm^2$.

Detection Limits and Experimental Sensitivity. In order for this approach to be of general utility, its sensitivity must be well matched to the questions at hand. Many experiments, such as those looking at overexpressed or semipurified metalloproteins, may be well within the sample concentrations that were examined in the experiment depicted in Figure 2. Others, such as those in which low-relative-abundance metalloproteins within complex natural samples are interrogated, may have higher demands. The sensitivity of our technique was evaluated by assessing the minimal detectable levels of metalloproteins under the currently available experimental conditions.

In establishing experimentally the minimal detectable levels of metalloproteins, a dilution series of jack bean urease was run by loading a series of wells with 23, 7, 2.3, and 1.1 μg of the protein. The native Tris-glycine gel was then run, blotted to PVDF, and mapped by scanning XRF (Figure 4). Both nickel, the natural cofactor of this protein, and sulfur, which is mainly present in cysteine and methionine residues, were visualized. Selecting the protein bands in the map as regions-of-interest (ROIs) using MAPS software (43), the signal from the protein bands was compared with the background from a similar region away from any protein. The thresh-

old at which the signal surpassed three times the noise corresponded to 225 ng of protein (or 2.5 pmol) for sulfur, and 60 ng of protein (or 0.6 pmol) for nickel, reflecting the fact that our methods are more sensitive for nickel. Many factors affect this value, which is yet to be fully optimized. Trace metal contamination of the PVDF substrate and buffers may be further addressed. Additionally, the planned installation of a helium-filled sample chamber will reduce X-rays scattering off air that contributes to background through incomplete charge collection. It will also significantly reduce absorption of emitted low-energy X-rays and thus greatly improve the sensitivity of the instrument for low-Z elements, such as sulfur and phosphorus. The latter is important in determining the positions of phosphorylated proteins. It should be noted that comparison of identical urease samples directly applied to the PVDF membrane relative to those run through native-PAGE and blotted indicate that roughly 50% of the analyte metalloprotein may be lost during native-PAGE and blotting. While some losses are likely to be unavoidable, further optimization of electrophoretic methods, as discussed earlier, may reduce them. We have begun to investigate the effects of varying running voltage, temperature, and buffer systems. Future work is planned to

address, in a systematic manner, the many factors affecting the preservation of metal−protein complexes during electrophoresis and further improve the overall experimental sensitivity.

Analysis of Chromium Binding to Blood Serum Proteins. Metallopharmaceuticals and environmental pollutants introduce metals into biological systems, creating changes that we need better tools to characterize. In an *in vitro* study, we spiked blood serum with chromium(III) and chromium(VI) compounds to mimic its role as a pharmaceutical or environmental pollutant (Figure 5 and Figure 6) (*7, 8*). While native-PAGE performed on these samples showed poor protein migration (see Supporting Information), the addition of SDS appeared to cause minimum disruption to the chromium−protein interactions while allowing better migration of the protein bands. This is likely to be associated with the inert nature of Cr(III)−ligand bonds compared to those of more labile metal ions. Figure 5, panel a shows that the two main protein bands in minimally disruptive SDS-PAGE of albumin-depleted bovine serum are those of the monomer bovine serum albumin (BSA, ∼65 kDa) and the BSA dimer (∼130 kDa) linked by a disulfide bond formed by air oxidation of the single cysteine residue in each of the monomer units (*44*). Assignment of the latter band is supported by its partial reduction in the presence of a cellular reductant, glutathione (lanes 4 and 5 in Figure 5, panel a) and by its complete disappearance in the presence of a stronger reductant, dithiothreitol (5.0 mM, data not shown). The presence of Cr binding did not cause any obvious changes in the speciation of protein bands or the relative migration of the proteins on the gel (Figure 5, panel a).

The Cr distribution among separated proteins (Figure 5, panel b) differed markedly depending on the type of Cr compound used and the treatment conditions. No measurable Cr signals were observed in the unspiked sample, a sample spiked with Cr(VI) ($[CrO_4]^{2-}$, 1.0 mM) only, and a sample spiked with glutathione (GSH, 5.0 mM) only (lanes 1, 3, and 4, respectively, Figure 5, panel b). This lack of significant binding of $[CrO_4]^{2-}$ to most biological macromolecules in the absence of strong reductants, except for the electrostatic binding to positively charged proteins such as histones, is in agreement with the literature data (*11, 45*). Reduction of Cr(VI) (1.0 mM) to Cr(III) with GSH (5.0 mM) (*45*) in the presence of serum proteins caused significant
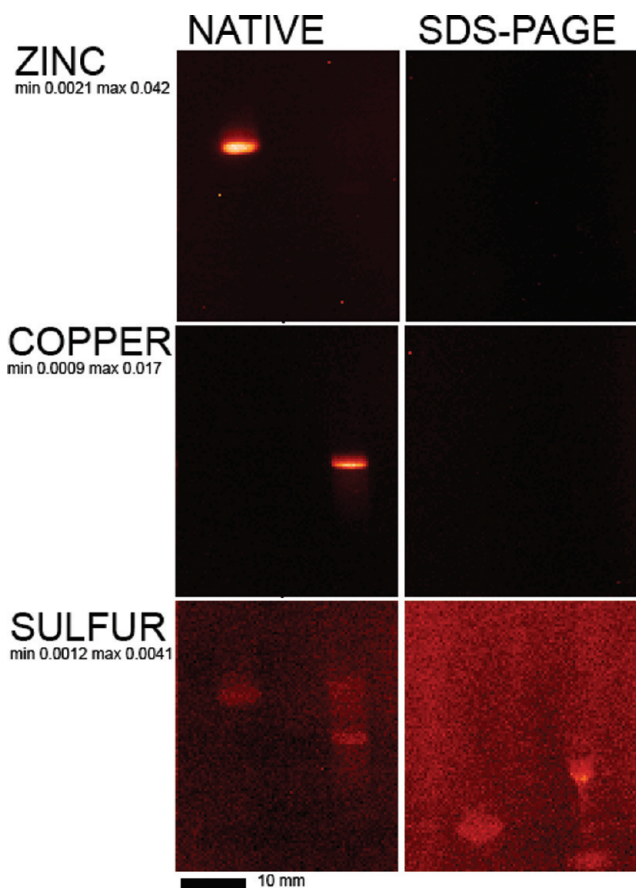

Figure 3. Separation by native-PAGE preserves metal content, whereas conventional SDS-PAGE does not. Identical samples of carbonic anhydrase (50 μg) and tyrosinase (50 μg) were run either by native-PAGE (left panels) or SDS-PAGE according to the method of Laemmli (*61*) (right panels), blotted, and mapped at the same time. Zinc and copper are present in carbonic anhydrase and tyrosinase, respectively, under native conditions but not following conventional SDS-PAGE. The bottom panels display the sulfur content, clearly showing that similar levels of protein are present in both samples.

Cr−protein binding (primarily to the BSA band, lane 5 in Figure 5, panel b), in agreement with the literature data on the formation of protein−Cr(III)−GSH crosslinks under these conditions (*46*), although it could also be due to the reduction of the disulfide to the thiol, which could then bind to Cr(VI) or Cr(V) en route to forming inert Cr(III) BSA species by similar mechanisms as observed for GSH reactions (*11, 47, 48*). By contrast, the reaction of serum proteins with the preformed Cr(III)−GSH complexes (products of Cr(VI) reduction with GSH) under the same conditions caused signifi-
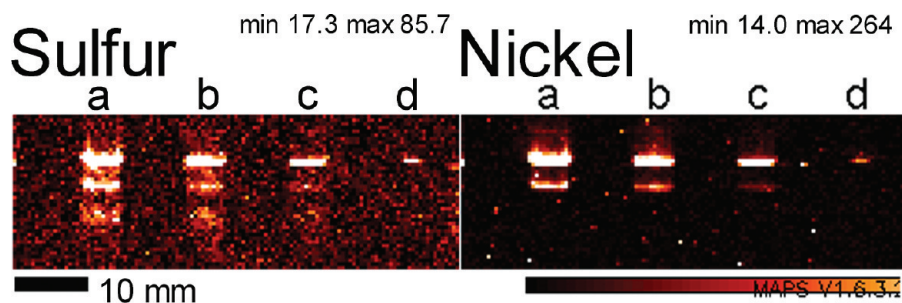
Figure 4. XRF map of a separation of urease for sensitivity measurements. Letters a, b, c, and d denote lanes with 23, 7, 2.3, or 1 μg of protein, respectively. (Left) Sulfur map shows sensitivity of this technique for the sulfur component of amino acids. (Right) Nickel map shows sensitivity of the technique in response to decreasing analyte concentration. The wide dynamic range of our data is not well rendered in an 8/24-bit image; for this view the upper and lower threshold values have been adjusted to optimally display the low intensity information. Images are displayed as total counts.

cantly lower Cr−protein binding, which occurs primarily in the high-MW region (lane 6 in Figure 5, panel b). This difference is consistent with the formation of reactive species (Cr(V/IV) complexes and/or reactive Cr(III) inter-

Figure 5. Protein map (a) and Cr map (b) for Cr compounds binding to albumin-depleted bovine serum proteins. The main protein bands at ~65 and ~130 kDa correspond to monomeric and dimeric forms of BSA, respectively (44), total protein content in each lane is ~10 μg. Lane 1: no Cr compounds added. Lane 2: $[Cr^{III}(OH_2)_6](NO_3)_3$ (1.0 mM). Lane 3: $Na_2Cr^{VI}O_4$ (1.0 mM). Lane 4: GSH (5.0 mM), no Cr added. Lane 5: $Na_2Cr^{VI}O_4$ (1.0 mM) + GSH (5.0 mM). Lane 6: Cr(III)-GSH complex (1.0 mM, generated by the reaction of 10 mM $Na_2Cr^{VI}O_4$ with 50 mM GSH in water at pH ~7 for 2 h at 310 K immediately prior to the addition to serum proteins) (45, 46); Lane 7: $[Cr_3^{III}O(OCOC_2H_5)_6(OH_2)_6](NO_3)$ (Cr(III)-propionate, 1.0 mM). All Cr compounds were incubated with serum proteins (1.0 mg protein per mL in 20 mM HEPES buffer, pH 7.4) for 2 h at 310 K prior to the separation by SDS-PAGE.

mediates) during the reduction of Cr(VI) in biological systems, which are thought to be responsible primarily for the toxicity and carcinogenicity of Cr(VI) (11, 14, 15, 45, 49).

The capacity of Cr(III) complexes (particularly those containing reactive aqua ligands) to bind to proteins was further demonstrated for $[Cr(OH_2)_6](NO_3)_3$ and $[Cr_3O(OCOC_2H_5)_6(OH_2)_3](NO_3)$ (1.0 mM Cr, lanes 2 and 7, respectively, Figure 5, panel b). The former complex binds to proteins to a lower extent (probably due to its rapid hydrolysis with the formation of insoluble hydroxido complexes) (11, 14, 15) and primarily to the BSA band (lane 2, Figure 5, panel b), whereas the latter complex binds extensively to high-MW proteins (lane 7, Figure 5, panel b). These data are particularly notable with regard to the suggested use of $[Cr_3O(OCOC_2H_5)_6(OH_2)_3](NO_3)$ (Cr(III) propionate) as a supposedly safer alternative to a popular nutritional supplement, Cr(III) picolinate (50). This complex was reported to be stable in extracellular media and to enter cells unchanged, where it was postulated to act as a specific activator of insulin receptors in order to explain its antidiabetic activity (51). However, the data of Figure 5, panel b support our earlier findings (52) on the extensive binding of this and other Cr(III) complexes to blood serum proteins prior to Cr entering cells. The resultant Cr(III)−protein adducts are capable of reactions with H_2O_2 and other biological oxidants present in the blood serum (particularly under pathological conditions, such as inflammation or diabetes) with the formation of Cr(VI) (14, 15, 52, 53). The antidiabetic activities of these Cr(III) complexes can then be explained by the ac-
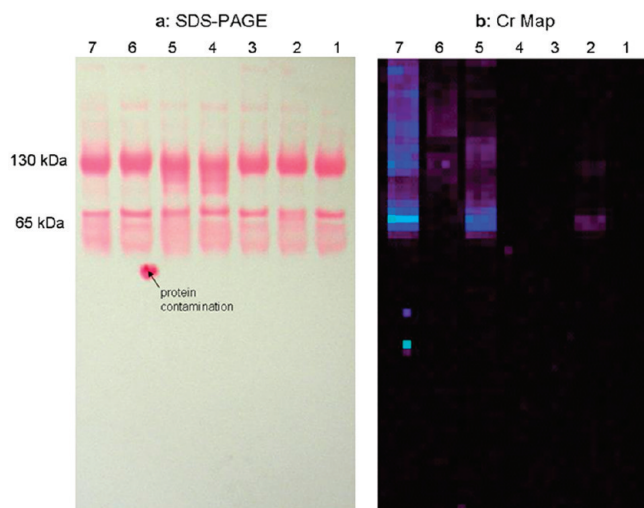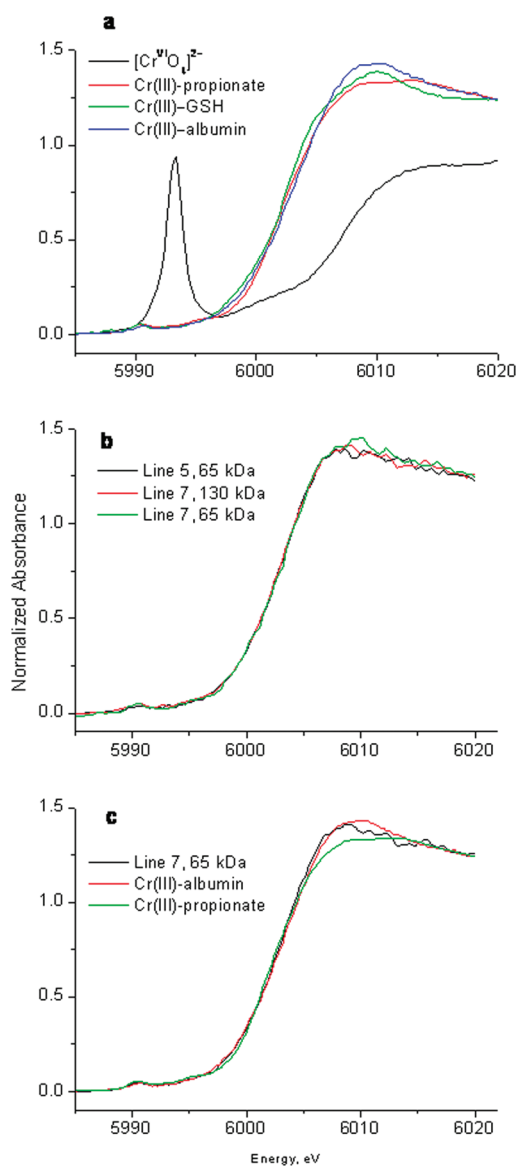
Figure 6. XANES spectra of Cr-containing protein bands on a PVDF membrane and model Cr compounds. Spectra of model Cr(VI) and Cr(III) compounds (*52, 54, 55*): a) typical XANES spectra of Cr-containing protein bands (corresponding to Figure 5panel b); b) comparison of a spectrum of a protein adduct (~65 kDa) formed during the reaction of Cr(III)-propionate with serum proteins (lane 7 in Figure 5, panel b) with those of the original Cr(III)-complex and c) a Cr(III)-albumin adduct (*52*).

tion of the resultant Cr(VI) as a nonspecific inhibitor of protein tyrosine phosphatases (which is similar in action to a well-known insulin-mimetic agent, V(V), which is

isoelectronic to Cr(VI) (*14, 15, 53*)). However, the chronic presence of low concentrations of Cr(VI) caused by long-term consumption of Cr(III) nutritional supplements is a matter of potential concern due to the well-known carcinogenicity of Cr(VI) (*11, 14, 15*). In summary, the results presented in Figure 5, panel b are consistent with our view of Cr(VI) toxicity and the antidiabetic action of Cr(III) as closely linked biological activities, involving the same reactive intermediates (*14, 15*).

The Cr(III)−-protein adducts detected by XRF mapping (Figure 5, panel b) were further analyzed by XAS (using the near-edge or XANES region, Figure 6), made possible by relatively high Cr contents in some protein bands. This analysis relied on the previously developed method of multiple linear regression analysis of XANES spectra of Cr(III) speciation in biological media, using libraries of spectra of model Cr(III) complexes (*52, 54*). Figure 6, panel a illustrates typical XANES spectra of model Cr compounds (*52, 54, 55*), with Cr(III) complexes obviously distinguished from Cr(VI) by lower edge energies and the absence of a sharp pre-edge feature at ~5993 eV (due to the 1s → 3d electronic transition) (*55*). There are also more subtle differences in the edge energies and postedge features of various Cr(III) complexes (*52, 54*), including increased absorbance at ~6010 eV for a Cr(III)−albumin adduct (prepared by the reaction of Cr(III)-propionate with the protein at pH 7.4, followed by the removal of unbound Cr(III) by membrane filtration) (*52*). Rat serum albumin was used for the published data (*52*), but a Cr(III)−BSA adduct prepared under the same conditions had a practically identical spectrum (A. Levina, unpublished results). Figure 6, panel b shows that similar XANES spectra were obtained for the reactions of serum proteins with either Cr(III) propionate or the Cr(VI) + GSH mixture (in the latter case, no measurable quantities of the oxidation states higher than Cr(III) were detected). Figure 6, panel c shows that the spectra of the resultant Cr(III)−protein adducts are closer to that of a previously reported Cr(III)−albumin adduct (*52*) than to those of the original complexes (e.g., Cr(III) propionate). These observations were supported by the results of multiple linear regression analysis (Supporting Information), which showed that the spectra of Cr(III) species in lanes 3 and 7 (Figure 5, panel b) were best fitted with a combination of those of a Cr(III)−albumin adduct (65−84%), Cr(III) amino acid complexes (12−28%, modeled as $[Cr(asp)_2]^-$, where asp = L-aspartato(2−))

(*54*), and Cr(III) hydroxido complexes (5−8%, modeled as $[Cr(OH)_6]^{3-}$) (*54*). Fitting results for the Cr(III) species found in the ∼65 kDa regions of both lanes 5 and 7 (Figure 5, panel b) were the same, within experimental error, while the fit for the species found in the ∼130 kDa region of lane 7 (Figure 5, panel b) was distinguished by a higher content of a coordination environment similar to the Cr(III)-albumin component (84 ± 2% vs 65 ± 2%, see Supporting Information). These results emphasize the possibility of Cr(III) binding to various functional groups of different proteins, which could not be detected in the previous studies (*52*). On the whole, the fitting results were similar to those obtained previously for the bulk samples of Cr(III) reaction products with blood serum (*52*), which confirms the suitability of the combination of XRF and XAS techniques for studies of MW distribution and chemical speciation of metal−protein complexes separated by gel electrophoresis.

Analysis of Iron in Cell Lysates. Purified proteins and *in vitro* systems present an ideal case for this analysis. Yet, natural biological samples are remarkably complex and are likely to contain numerous metalloproteins of widely varying relative abundance. One might ask, will this method work well in such cases?

In seeking an answer, we examined the facultative anaerobe *Shewanella oneidensis* MR-1. *S. oneidensis* MR-1, in the absence of oxygen, is capable of utilizing a diverse array of final electron acceptors, among them iron, chromium, plutonium, and uranium, through dissimilitory metabolism (*56*). These capabilities have made it of considerable interest for the remediation of radionuclide-contaminated sites. Reduction of some contaminants, such as U(VI), changes their environmental mobility such that movement into rivers and groundwater is minimized, and cleanup is facilitated (*57*). Although much work has been done to characterize the metabolism of this organism on both a systems (*56*) and proteomic level (*58, 59*), a fuller picture of the key players in its respiration of these metals would be useful for development of biotechnological applications. Some of the proteins upregulated by *S. oneidensis* MR-1 under anoxic conditions are known iron proteins (*58, 59*). To verify our ability to detect this change in endogenous
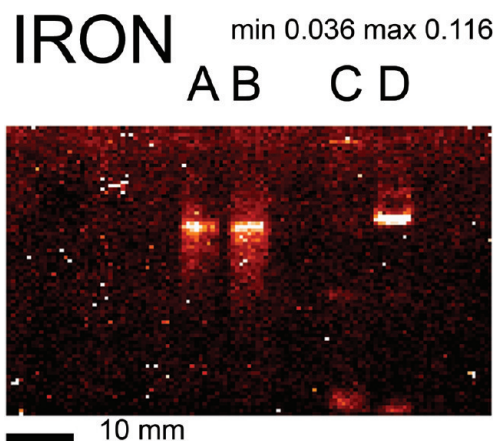

Figure 7. XRF map of a one-dimensional native-PAGE blot of *Shewanella oneidensis* lysates. (Lanes A and B) Positive control samples of hemoglobin. Lanes C and D: Lysates from aerobically (C) and anaerobically (D) grown *Shewanella oneidensis* MR-1. Maps displayed are quantified, with threshold values in μg cm^{-2}.

metalloprotein content, cell pellets from both oxygen-deficient and oxygen-replete cultures were lysed into native sample loading buffer. Following native-PAGE electrophoresis and blotting to PVDF, the lysates were mapped by XRF (Figure 7). While some faint bands of iron are detected in both samples, one of the iron bands is strongly present in only the anaerobic sample. This is consistent with published proteomics studies of MR-1, which found that several iron proteins of this mass are highly expressed only under anaerobic conditions (*59*). Though not possible from this 1-D separation, future work, utilizing 2-D gel electrophoresis and mass spectrometry, will begin to identify individual proteins involved. Yet, the novelty of this technique, in directly and quantitatively visualizing the iron itself, opens up new questions. For example, we may now ask, which of the proteins are responsible for binding most of the iron? How does this change with time? How does the iron:protein ratio change with the extent of oxygenation? Can we identify new iron proteins involved? Answers to questions such as these now lie much more readily within our grasp.

METHODS
Evaluation of Substrates for XRF. Substrates were evaluated by mapping strips of blotting membranes, including nylon, poly-

vinylidene fluoride (PVDF), and nitrocellulose from several manufacturers, including Osmonics, GE Healthcare, Millipore, and Exapure. Immobilon-PSQ PVDF (Millipore) was selected for

its relatively low X-ray fluorescence background at iron, copper, and zinc emission energies.

Electrophoresis of Purified Metalloproteins. Commercially available metalloproteins (all from Sigma), including bovine carbonic anhydrase (CA), bovine carbonic anhydrase isoform II (CAII), mushroom tyrosinase (Tyr), bovine hemoglobin (Hb), and jack bean urease (Ur) along with Novex Sharp prestained molecular weight marker (Invitrogen) or Kaleidoscope prestained standards (Bio-Rad) were variously subjected to discontinuous native polyacrylamide gel electrophoresis (native-PAGE) as described for each figure. Prior to gel separations, all equipment was thoroughly rinsed with Milli-Q water. The samples were applied as approximately 10 mg mL^{-1} solutions in Tris-Cl buffer, pH 6.8, to either 4−15% gradient Tris-Cl Ready Gels (Bio-Rad) or 4−20% Novex Tris-glycine mini gels (Invitrogen) and were subjected to electrophoresis at 100 V for 1 h in standard Tris-glycine running buffer (25 mM Tris, 192 mM glycine, pH 8.3; made with Milli-Q water) (60). After assembling the blotting cassette in a glass tray using only Teflon tweezers to manipulate the materials, gels were blotted to a PVDF membrane using a wet transfer system with Tris-glycine running buffer, at 0.35 A for 1 h. Blots were then gently rinsed in the same buffer, carefully dried free from dust, and stored covered prior to mapping.

In one experiment, for the purpose of comparison, native-PAGE of 50 μg of tyrosinase and 50 μg of carbonic anhydrase was run as above, while in parallel, equal amounts of each protein were run using standard SDS-PAGE techniques according to the method of Laemmli (61).

Preparation of Chromium-Exposed Serum Samples and Their Separation by SDS-PAGE. Albumin-depleted bovine serum was prepared using Affi-Gel Blue columns from Bio-Rad (resin volume, ∼2 mL). Cell-culture-grade fetal calf serum from Invitrogen (0.10 mL) was diluted with a low-salt buffer (0.30 mL, 20 mM HEPES, pH 7.4) and passed through an equilibrated column. The column was then eluted with the low-salt buffer (0.40 mL), and the eluate was diluted to 1.0 mg mL^{-1} protein using the same buffer. Determination of the protein content in dilute solutions was performed by the Bradford method, using bovine serum albumin (BSA, Sigma) as a standard. Stock solutions of Cr(VI) or Cr(III) compounds (1.0 μL, 10 mM Cr) and/or glutathione (GSH, 50 mM, 1.0 μL) were added to the dilute serum solutions (10 μL), which were then incubated for 2 h at 37 °C. The reactions were stopped by cooling the reaction mixtures to 0 °C followed by the addition of a sample buffer (3.0 μL, Nu-PAGE, from Invitrogen), after which the samples were loaded into a 1-mm thick NuPAGE 4−12% bis-Tris gel (Invitrogen). Native-PAGE was run as described above for purified proteins. A minimally disruptive variation of SDS-PAGE and blotting of proteins to a PVDF membrane were performed using the Novex mini-gel system and blot module according to the manufacturer's instructions (62), except that the running buffer (50 mM MES, 50 mM Tris, 0.1% SDS, pH 7.3) and the transfer buffer (25 mM bicine, 25 mM bis-Tris, pH 7.3) did not contain EDTA or other strong complexants, including reducing agents, and the samples were not heated. All of these factors are important in order to prevent the cleavage of metal ions from the protein complexes. Molecular weights (MW) of the proteins were determined using the SeeBlue Plus2 prestained standard from Invitrogen. Two parallel gels were run for each experiment, and one of the resulting PVDF membranes was stained with a Ponceau S dye solution (Sigma) for 15 min for protein visualization, while the second membrane was left unstained for elemental mapping.

Cell Lysate Preparation and Electrophoresis. The facultative anaerobe *Shewanella oneidensis* MR-1 was cultured under both high and low oxygen conditions as previously described (59). The pellets were thawed on ice, and 0.6 mg of each pellet was suspended into 60 μL of standard 2x native loading buffer (60).

The pellets were then lysed with three cycles of freezing and thawing. Cell debris was pelleted by centrifugation in a microcentrifuge at 13,000*g* for 2 min. Ten microliters of each supernatant was loaded onto a Novex 4−20% Tris-glycine native-PAGE gel (Invitrogen) next to lanes of molecular weight marker (MW; Novex Sharp Prestained protein marker, Invitrogen), and 10 μg each of carbonic anhydrase (CA), hemoglobin (Hb), and tyrosinase (Tyr), all from Sigma, and a mixture of 10 μg of each of these three proteins. The native gel was run and blotted as described above for purified metalloproteins.

X-ray Fluorescence Scanning. Scanning was performed in air using the instrument shown (Figure 1) at beamline 2-ID-E of Sector 2 at the Advanced Photon Source (APS). This instrument has now been placed at a permanent home at beamline 8-BM of Sector 8, where it is publicly available through the general user proposal system. Undulator generated hard X-rays (10.0 keV) were monochromatized and passed through a pinhole (spot diameter on sample, 0.5 mm). Full X-ray fluorescence spectra were collected at each raster-scan step using a single element silicon drift detector (Vortex EX, SII NanoTechnology). Spectra were fitted against NIST standards NBS1832 and NBS1833 using per-pixel peak fitting algorithms with MAPS software (43). This fitting creates maps of the gel specific for each element of the periodic table with atomic numbers ranging from phosphorus ($Z = 15$) to zinc ($Z = 30$), with spatial resolution limited by the beam spot size, as well as the chosen sampling. Scanning of an entire mini-gel blot typically took between 4−8 h depending on pixel resolution and dwell times. For X-ray absorption near edge spectroscopy (XANES), selected protein bands were cut out of PVDF membranes mapped previously at 2-ID-E. XANES spectra were then acquired at beamline 2-ID-D of the APS using a millimeter-sized beam, monochromatized by a silicon ⟨111⟩ double crystal monochromator (Kohzu Precision). XAS were acquired in fluorescence mode with a silicon drift detector (Vortex, SII NanoTechnology), 2s dwell time per pixel, and 0.5-eV steps. The XAS data were processed with the use of XFit (63) and Origin (64) software, as well as libraries of spectra of model Cr(III) compounds, as described previously (52, 54).

Metal:Protein Ratio Determination. The protein concentration of each sample was measured by Quant-IT protein assay (Invitrogen) using a microplate reader. For ICP-AES, stock samples of each protein standard were diluted approximately 1:1000 into Milli-Q water that was acidified with ultrapure nitric acid and analyzed using a Thermo-Jarrell Ash inductively coupled plasma atomic emission (ICP-AES) spectrometer relative to a manual one-point standardization. Additionally, stock solutions of proteins were blotted onto PVDF directly in a dot blot for quantification of the concentration of metals in the samples prior to electrophoresis by XRF. These dot blots were mapped by XRF in a manner identical to that employed for the blotted gels. The quantity of metal in the protein bands was determined by integration of the fitted fluorescence data for a metal of interest over an area corresponding to the protein band, with subtraction of background fluorescence intensity integrated at the same energy over the same area. The ratios of metal to protein in the samples prior to electrophoresis were determined both by comparison of the ICP-AES data to the protein concentration, as well as independent comparison of the XRF dot blot analysis to the protein concentration. XRF measurements of the dot-blotted protein and ICP-AES of the same solution produced similar results.

REFERENCES

1. Bertini, I., Gray, H. B., Stiefel, E. I., and Valentine, J. S., Eds. (2007) *Biological Inorganic Chemistry: Structure and Reactivity*, University Science Books, Sausalito, CA.

2. Finney, L. A., and O'Halloran, T. V. (2003) Transition metal speciation in the cell: insights from the chemistry of metal ion receptors, *Science 300*, 931–936.

3. Tottey, S., Waldron, K. J., Firbank, S. J., Reale, B., Bessant, C., Sato, K., Cheek, T. R., Gray, J., Banfield, M. J., Dennison, C., and Robinson, N. J. (2008) Protein-folding location can regulate manganese-binding versus copper- or zinc-binding, *Nature 455*, 1138–1142.

4. Finney, L., Mandava, S., Ursos, L., Zhang, W., Rodi, D., Vogt, S., Legnini, D., Maser, J., Ikpatt, F., Olopade, O. I., and Glesne, D. (2007) X-ray fluorescence microscopy reveals large-scale relocalization and extracellular translocation of cellular copper during angiogenesis, *Proc. Natl. Acad. Sci. U.S.A. 104*, 2247–2252.

5. Witting, P. K., Harris, H. H., Rayner, B. S., Aitken, J. B., Dillon, C. T., Stocker, R., Lai, B., Cai, Z., and Lay, P. A. (2006) The endothelium-derived hyperpolarizing factor, H_2O_2, promotes metal-ion efflux in aortic endothelial cells: elemental mapping by a hard X-ray microprobe, *Biochemistry 45*, 12500–12509.

6. Duong, T. T., Witting, P. K., Antao, S. T., Parry, S. N., Kennerson, M., Lai, B., Vogt, S., Lay, P. A., and Harris, H. H. (2009) Multiple protective activities of neuroglobin in cultured neuronal cells exposed to hypoxia re-oxygenation injury, *J. Neurochem. 108*, 1143–1154.

7. Reedijk, J. (2009) Medicinal applications of metal complexes binding to biological macromolecules, *Macromol. Symp. 270*, 193–201.

8. Stefanidou, M., and Maravelias, C. (2004) Metallothioneins in toxicology, *Curr. Top. Toxicol. 1*, 161–167.

9. Liu, M., Lim, Z. J., Gwee, Y. Y., Levina, A., and Lay, P. A. (2010) Characterization of ruthenium (III)/ NAMI-A adduct with bovine serum albumin that exhibits a high anti-metastatic activity, *Angew. Chem., Int. Ed. 49*, 1661–1664.

10. Levina, A., Mitra, A., and Lay, P. A. (2009) Mechanisms for the biological activities of ruthenium anticancer drugs, *Metallomics 1*, 458–470.

11. Levina, A., Codd, R., Dillon, C. T., and Lay, P. A. (2003) Chromium in biology: toxicology and nutritional aspects, *Prog. Inorg. Chem. 51*, 145–200.

12. *Overall Evaluation of Carcinogenicity to Humans*, International Agency for Research on Cancer, Lyon, France, http://www.iarc.fr.

13. Institute of Medicine, Food and Nutrition Board (2001) *Dietary Reference Intakes for Vitamin A, Vitamin K, Arsenic, Boron, Chromium, Copper, Iodine, Iron, Molybdenum, Nickel, Silicon, Vanadium, and Zinc*, National Academy Press, Washington, DC.

14. Levina, A., and Lay, P. A. (2008) Chemical properties and toxicity of chromium(III) nutritional supplements, *Chem. Res. Toxicol. 21*, 563–571.

15. Levina, A., Mulyani, I., Lay, P. A. (2007) Redox chemistry and biological activities of chromium(III) complexes, in *The Nutritional Biochemistry of Chromium(III)* (Vincent, J. B., Ed.) pp 225–256, Elsevier, Amsterdam.

16. Garcia, J. S., de Magalhaes, C. S., and Arruda, M. A. Z. (2006) Trends in metal-binding and metalloprotein analysis, *Talanta 69*, 1–15.

17. Szpunar, J. (2005) Advances in analytical methodology for bioinorganic speciation analysis: metallomics, metalloproteomics and heteroatom-tagged proteomics and metabolomics, *Analyst 130*, 442–465.

18. Becker, J. S., Zoriy, M. V., Pickhardta, C., and Zillesb, K. (2005) Copper, zinc, phosphorus and sulfur distribution in thin section of rat brain tissues measured by laser ablation inductively coupled plasma mass spectrometry: possibility for small-size tumor analysis, *J. Anal. At. Spectrom. 20*, 912–917.

19. Chery, C. C., Gunther, D., Cornelis, R., Vanhaecke, F., and Moens, L. (2003) Detection of metals in proteins by means of polyacrylamide gel electrophoresis and laser ablation-inductively coupled plasma-mass spectrometry: application to selenium, *Electrophoresis 24*, 3305–3313.

20. Ma, R., McLeod, C. W., Tomlinson, K., and Poole, R. K. (2004) Speciation of protein-bound trace elements by gel electrophoresis and atomic spectrometry, *Electrophoresis 25*, 2469–2477.

21. Neilsen, J. L., Abildtrup, A., Christensen, J., Watson, P., Cox, A., and McLeod, C. W. (1998) Laser ablation inductively coupled plasma-mass spectrometry in combination with gel electrophoresis: a new strategy for speciation of metal binding serum proteins, *Spectrochim. Acta Part B 53*, 339–345.

22. Marshall, P. S., Leavens, B., Heudi, O., and Ramirez-Molina, C. (2004) Liquid chromatography coupled with inductively coupled plasma mass spectrometry in the pharmaceutical industry: selected examples, *J. Chromatogr. A 1056*, 3–12.

23. Becker, J. S., Lobinski, R., and Becker, J. S. (2009) Metal imaging in non-denaturing 2D electrophoresis gels by laser ablation inductively coupled plasma mass spectrometry (LA-ICP-MS) for the detection of metalloproteins, *Metallomics 1*, 312–316.

24. Paunesku, T., Vogt, S., Maser, J., Lai, B., and Woloschak, G. (2006) X-ray fluorescence microprobe imaging in biology and medicine, *J. Cell. Biochem. 99*, 1489–1502.

25. Aitken, J. B., Carter, E. A., Eastgate, H., Hackett, M. J., Harris, H. H., Levina, A., Lee, Y.-C., Chen, C.-I., Lai, B., Vogt, S., and Lay, P. A. (2010) Biomedical applications of X-ray absorption and vibrational spectroscopic microscopies in obtaining structural information from complex systems, *Radiat. Phys. Chem. 79*, 176–184.

26. Dong, Y., Gao, Y. X., Chen, C. Y., Li, B., Li, X., Yu, H. W., He, W., Huang, Y. Y., and Chai, Z. F. (2006) Quantification of trace elements in protein bands using synchrotron radiation X-ray fluorescence after electrophoretic separation, *Chin. J. Anal. Chem. 34*, 443–446.

27. Gao, Y. X., Chen, C. Y., Chai, Z. F., Zhao, J. J., Liu, J., Zhang, P. Q., He, W., and Huang, Y. Y. (2002) Detection of metalloproteins in human liver cytosol by synchrotron radiation X-ray fluorescence combined with gel filtration chromatography and isoelectric focusing separation, *Analyst 127*, 1700–1704.

28. Kemner, K. M., Kelly, S. D., O'Loughlin, E. J., T., K., Moe, L. A., Fox, B. G., Donnelly, M. I., Londer, Y., Schiffer, M., and Giometti, C. S. (2005) XRF and XAFS analysis of electrophoretically isolated nondenatured proteins, *Phys. Scr. T115*, 940–942.

29. Liu, Y. B., Gao, Y. X., Chen, C. Y., Li, B., Yu, H. W., Wang, J. X., He, W., Huang, Y. Y., and Chai, Z. F. (2005) Quantitative analysis of iron in protein bands existing in polyacrylamide gel matrix with synchrotron radiation X-ray fluorescence, *High Energy Phys. Nucl. Phys.–Chin. Ed. 29*, 61–64.

30. Garcia, J. S., da Silva, G. A., Arruda, M. A. Z., and Poppi, R. J. (2007) Application of Kohonen neural network to exploratory analyses of synchroton radiation X-ray fluorescence measurements of sunflower metalloproteins, *X-Ray Spectrum. 36*, 122–129.

31. Kuhbacher, M., Weseloh, G., Thomzig, A., Bertelsmann, H., Falkenberg, G., Radtke, M., Riesemeier, H., Kyriakopoulos, A., Beekes, M., and Behne, D. (2005) Analysis and localization of metal- and metalloid-containing proteins by synchrotron radiation X-ray fluorescence spectrometry, *X-Ray Spectrum. 34*, 112–117.

32. Sussulini, A., Garcia, J. S., Mesko, M. F., Moraes, D. P., Flores, E. M. M., Perez, C. A., and Arruda, M. A. Z. (2007) Evaluation of soybean seed protein extraction focusing on metalloprotein analysis, *Microchim. Acta 158*, 173–180.

33. Verbi, F. M., Arruda, S. C., Rodriguez, A. P., Perez, C. A., and Arruda, M. A. (2005) Metal-binding proteins scanning and determination by combining gel electrophoresis, synchrotron radiation X-ray fluorescence and atomic spectrometry, *J. Biochem. Biophys. Methods 62*, 97–109.

34. Weseloh, G., Kuhbacher, M., Bertelsmann, H., Ozaslan, M., Kyriako-poulos, A., Knochel, A., and Behnel, D. (2004) Analysis of metal-containing proteins by gel electrophoresis and synchrotron radiation X-ray fluorescence, *J. Radioanal. Nucl. Chem. 259*, 473–477.

35. Chevreux, S., Roudeau, S., Fraysse, A., Carmona, A., Deves, G., Solari, P. L., Mounicou, S., Lobinski, R., and Ortega, R. (2009) Multimodal analysis of metals in copper-zinc superoxide dismutase isoforms separated on electrophoresis gels, *Biochimie 91*, 1324–1327.

36. Ascone, I., Fourme, R., Hasnain, S., and Hodgson, K. (2005) Metallogenomics and biological X-ray absorption spectroscopy, *J. Synch. Rad. 12*, 1–3.

37. Mann, S. E., Ringo, M. C., Shea-McCarthy, G., Penner-Hahn, J., and Evans, C. E. (2000) Element-specific detection in capillary electrophoresis using X-ray fluorescence spectroscopy, *Anal. Chem. 72*, 1754–1758.

38. Scott, R. A., Shokes, J. E., Cosper, N. J., Jenney, F. E., and Adams, M. W. (2005) Bottlenecks and roadblocks in high-throughput XAS for structural genomics, *J. Synch. Rad. 12*, 19–22.

39. Haraguchi, H. (1999) Multielement profiling analyses of biological, geochemical, and environmental samples as studed by analytical atomic spectrometry, *Bull. Chem. Soc. Jpn. 72*, 1163–1186.

40. Szpunar, J. (2000) Bio-inorganic speciation analysis by hyphenated techniques, *Analyst 125*, 963–988.

41. Lippard, S. J.,and Berg, J. M. (1994) *Principles of Bioinorganic Chemistry*, University Science Books, Mill Valley, CA.

42. Hu, W., Luo, Q., Ma, X., Wu, K., Liu, J., Chen, Y., Xiong, S., Wang, J., Sadler, P. J., and Wang, F. (2009) Arene control over thiolate to sulfinate oxidation in albumin by organometallic ruthenium anticancer complexes, *Chemistry 15*, 6586–6594.

43. Vogt, S. (2003) MAPS: a set of software tools for analysis and visualization of 3D X-ray fluorescence data sets, *J. Phys. IV 104*, 635–638.

44. Scorza, G., and Minetti, M. (1998) One-electron oxidation pathway of thiols by peroxynitrite in biological fluids: bicarbonate and ascorbate promote the formation of albumin disulphide dimers in human blood plasma, *Biochem. J. 329*, 405–413 (Pt 2).

45. Levina, A., and Lay, P. A. (2005) Mechanistic studies of relevance to the biological activities of chromium, *Coord. Chem. Rev. 249*, 281–298.

46. Guttmann, D., Poage, G., Johnston, T., and Zhitkovich, A. (2008) Reduction with glutathione is a weakly mutagenic pathway in chromium(VI) metabolism, *Chem. Res. Toxicol. 21*, 2188–2194.

47. Levina, A., and Lay, P. A. (2004) Solution structures of chromium(VI) complexes with glutathione and model thiols, *Inorg. Chem. 43*, 324–335.

48. Levina, A., Zhang, L., and Lay, P. A. (2003) Structure and reactivity of a chromium(V) glutathione complex, *Inorg. Chem. 42*, 767–784.

49. Zhitkovich, A. (2005) Importance of chromium-DNA adducts in mutagenicity and toxicity of chromium(VI), *Chem. Res. Toxicol. 18*, 3–11.

50. Vincent, J. B., and Davis, C. M.Use of triaqua-μ^3-oxohexakis-*m*-propionatotrichromium (1+), [Cr$_3$O(O$_2$CCH$_2$CH$_3$)$_6$(H$_2$O)$_3$]$^+$, as a nutritional supplement or in treatment of medical conditions, U.S. Patent 6,197,816, 2001.

51. Shute, A. A., Chakov, N. E., and Vincent, J. B. (2001) The stability of the biomimetiation triaqua-*m*-oxohexaproprionatotrichromium(III) *in vivo* in rats, *Polyhedron 20*, 2241–2252.

52. Nguyen, A., Mulyani, I., Levina, A., and Lay, P. A. (2008) Reactivity of chromium(III) nutritional supplements in biological media: an X-ray absorption spectroscopic study, *Inorg. Chem. 47*, 4299–4309.

53. Mulyani, I., Levina, A., and Lay, P. A. (2004) Biomimetic oxidation of chromium(III): does the antidiabetic activity of chromium(III) involve carcinogenic chromium(VI)? *Angew. Chem., Int. Ed. 43*, 4504–4507.

54. Levina, A., Harris, H. H., and Lay, P. A. (2007) X-ray absorption and EPR spectroscopic studies of the biotransformations of chromium(VI) in mammalian cells. Is chromodulin an artifact of isolation methods? *J. Am. Chem. Soc. 129*, 1065–1075.

55. Harris, H. H., Levina, A., Dillon, C. T., Mulyani, I., Lai, B., Cai, Z., and Lay, P. A. (2005) Time-dependent uptake, distribution and biotransformation of chromium(VI) in individual and bulk human lung cells: application of synchrotron radiation techniques, *J. Biol. Inorg. Chem. 10*, 105–118.

56. Fredrickson, J. K., Romine, M. F., Beliaev, A. S., Auchtung, J. M., Driscoll, M. E., Gardner, T. S., Nealson, K. H., Osterman, A. L., Pinchuk, G., Reed, J. L., Rodionov, D. A., Rodrigues, J. L., Saffarini, D. A., Serres, M. H., Spormann, A. M., Zhulin, I. B., and Tiedje, J. M. (2008) Towards environmental systems biology of *Shewanella*, *Nat. Rev. Microbiol. 6*, 592–603.

57. Hau, H. H., and Gralnick, J. A. (2007) Ecology and biotechnology of the genus *Shewanella*, *Annu. Rev. Microbiol. 61*, 237–258.

58. Kolker, E., Picone, A. F., Galperin, M. Y., Romine, M. F., Higdon, R., Makarova, K. S., Kolker, N., Anderson, G. A., Qiu, X., Auberry, K. J., Babnigg, G., Beliaev, A. S., Edlefsen, P., Elias, D. A., Gorby, Y. A., Holzman, T., Klappenbach, J. A., Konstantinidis, K. T., Land, M. L., Lipton, M. S., McCue, L. A., Monroe, M., Pasa-Tolic, L., Pinchuk, G., Purvine, S., Serres, M. H., Tsapin, S., Zakrajsek, B. A., Zhu, W., Zhou, J., Larimer, F. W., Lawrence, C. E., Riley, M., Collart, F. R., Yates, J. R., 3rd, Smith, R. D., Giometti, C. S., Nealson, K. H., Fredrickson, J. K., and Tiedje, J. M. (2005) Global profiling of *Shewanella oneidensis* MR-1: expression of hypothetical genes and improved functional annotations, *Proc. Natl. Acad. Sci. U.S.A. 102*, 2099–2104.

59. Giometti, C. S., Khare, T., Tollaksen, S. L., Tsapin, A., Zhu, W. H., Yates, J. R., and Nealson, K. H. (2003) Analysis of the *Shewanella oneidensis* proteome by two-dimensional gel electrophoresis under 3 nondenaturing conditions, *Proteomics 3*, 777–785.

60. Coligan, J., Dunn, B, Speicher, D., and Wingfield, P., Eds. (2008) *Current Protocols in Protein Science*, John Wiley and Sons, Edison, NJ.

61. Laemmli, U. K. (1970) Cleavage of structural proteins during the assembly of the head of bacteriophage T4, *Nature 227*, 680–685.

62. Invitrogen (2003) Novex Pre-Cast Gel Electrophoresis Guide, Version B.

63. Australian Synchrotron Research Program (2004) XFit for Windows, beta-version.

64. OriginLab Corporation (1999). Microcal Origin (6.0).